Practicality of methyl acetate as a co-solvent for fast charging Na-ion battery electrolytes

Parth Desai, John Abou-Rjeily, Jean-Marie Tarascon, Mariyappan Sathiya

Practicality of methyl acetate as a co-solvent for fast charging Na-ion battery electrolytes

Parth Desai,[1,2,3] John Abou-Rjeily,[3,4] Jean-Marie Tarascon[1,2,3], and Sathiya Mariyappan,[1,3]*

[1]Chimie du Solide-Energie, UMR 8260, Collège de France, 75231 Paris Cedex 05, France

[2]Sorbonne Université, 4 Place Jussieu, 75005, Paris, France

[3]Réseau sur le Stockage Electrochimique de l'Energie (RS2E), FR CNRS 3459, France

[4]TIAMAT energy, Hub de l'énergie, rue Baudelocque, 80000 Amiens, France

*Corresponding author: sathiya.mariyappan@college-de-france.fr

Keywords: Low temperature electrolyte, Fast charging battery, Sodium-ion battery, Methyl acetate co-solvent, Sodium plating

Abstract

Rapid research and technological improvements on Na-ion batteries (NIBs) are making them the most practicable complementary device for lithium-ion batteries (LIBs). Moreover, the high Na-ion diffusion kinetics offers several fast charging electrode materials that are attractive for high power applications. Lowering interphase and charge transfer resistances via innovative electrolytes design, while not scarifying lifetime, is however essential to secure such applications. Herein, we report the effect of low viscous ester based co-solvents in improving the conductivity of Na-ion based electrolyte. Our new electrolyte formulation shows excellent power capability charging the 18650 cell to 84% state of charge (SOC) within ~10 minutes. Additionally it improved low temperature cyclability, but with a slightly reduced high temperature performance against our co-solvent free electrolyte. We believe that the guideline taken here will pave the way towards finding a better compromise between ultrafast charging and high temperature applications for reaching optimum performance.

1. Introduction

In recent times, lithium-ion batteries (LIBs) are playing a pivotal role in the electrification of transportation and in enabling smarter power grids[1–4]. Improvements in the manufacturing technology and supply-chain establishment have reduced the cost of LIBs from over $1000/kWh to around $200/kWh[5]. However, manufacturing

advancements are reaching their limits[5,6] and a sudden upsurge in prices of lithium-based precursors[7,8] questions electrochemical energy storage solely depending on Li-based batteries. Moreover, the growing demand for low-cost batteries raises concerns about the availability and geopolitical independence of lithium resources[6,9]. To this end, sodium-ion batteries (NIBs) are emerging as attractive complementary energy storage devices because of the low cost and demographic neutrality of sodium precursors[9,10].

Further, fast-charging (FC) is the new Holy Grail in the advancement of battery technology. In 2018, the US Department of Energy released over $19 million in funding to enable ultrafast charging (XFC) with the goal of charging EV's in only 15min or less by 2028[11]. In this context, the Na-ion batteries can gain more importance as some of the Na-ion electrodes and electrolytes are reported to exhibit faster Na-ion diffusion kinetics than their lithium counterpart[12]. Especially, the positive electrodes such as $Na_3V_2(PO_4)_2F_3$ (NVPF)[13] and Prussian blue analogs (PBA)[14] are capable of (de)inserting sodium at a rate of, as fast as 10C (full capacity in 6 minutes). On the other side, the most commonly used Na-ion negative electrode hard carbon (HC) exhibit indirectly better rate capability than the Li-counterpart graphite due to its slightly higher redox potential[15]. The higher redox potential of hard carbon allows Na-insertion at faster rate without leading to a competing Na-plating process.

As important as both positive and negative electrode, the electrolyte transport properties that play a decisive role in determining how fast a cell can be charged. The polarization across the electrolyte and at the electrode-electrolyte interphase, particularly at low temperatures and/or high rates, can result in limited deployable capacity due to an early hitting of the cut-off voltage[16,17]. The more pronounced effect of fast charging is a reduction in calendar/cycle lifetimes and in some extreme cases rollover failure. In LIBs, the rollover behavior is attributed to unwanted lithium plating on the negative electrode surface when large currents are applied[18,19]. Lifetime loss due to plating occurs via multifold routes[20–22]. Firstly, the plated metal results from consuming the cell's active metal ion (Li^+/ Na^+) inventory, leading to irreversible capacity loss. Secondly, the plated metal is not chemically stable and reacts with electrolyte releasing byproduct gases and forming new solid-electrolyte interphase

(SEI). Finally, in some extreme cases, this plated metal can form dendrites and create shorts in the cell, raising some safety concerns.

Considering the Na-ion electrolytes, high Na-ion conductivity is reported due to weaker solvation of the Na^+-ion as compared to Li^+-ion[23]. However, the interphase formed is often reported to be poorly stable and necessitates the usage of electrolyte additives that can increase the interphase resistance that in turn reduce the power rate capability[24,25]. Hence, to achieve FC Na-ion cells, the electrolyte design needs, besides having high ionic conductivity, to form both highly conductive and stable interphases over a wide temperature range.

One way reported with LIBs to enable FC is to engineer electrode material with coatings or smaller particle sizes that increase electrical and Li^+ conductive transport in the material[26–29]. Another approach is to use salts/additives[30,31] like Lithium bis(fluorosulfonyl)imide (LiFSI), Lithium bis(trifluoromethanesulfonyl)imide (LiTFSI) etc. that reduces the interphase resistance. Finally, to circumvent the polarization (and plating) issue and enable FC is to increase the ionic conductivity of the electrolyte by incorporating low viscosity ester based co-solvents[32–38]. It has been claimed that ester based co-solvents help to reduce the depletion of Li^+ at the negative electrode surface during insertion, hence decreasing the overpotential and consequently avoiding associated metal plating during applied high currents[37,39–41]. However, the major disadvantage of the organic ester based co-solvents is their poor electrochemical stability. Therefore, in the present study, we explored the impact of adding methyl acetate (MA) and/or ethyl acetate on the Na-ion electrolyte's conductivity and electrochemical performance of our reference electrolyte containing 4 additives namely sodium oxalato(difluoro)borate (NaODFB), vinylene carbonate (VC), succinonitrile (SN), and tris-trimethylsilylphosphite (TMSPi). These additives form a good passivation film and lead to good performance at room temperature and high temperature[42]. With the incorporation of MA the charge transfer resistance is significantly reduced, thus less polarization and greater capacity are achieved at low temperatures (0 °C). Finally, 18650 Na-ion NVPF/HC assembled with up to 20% of MA exhibited 84% of their full capacity at 5C rate (full charge in 10-11 minutes). However, this co-solvent is still not

perfect as it induces some lifetime penalties at high temperatures as compared to a co-solvent free electrolyte containing additives.

2. Experimental

Ionic conductivity measurements: Bulk ionic conductivity of the electrolyte solutions was measured using a Mettler Toledo S230 conductivity meter. For accurate measurements, the conductivity meter was calibrated using a known standard solution of conductivity 12.88 mS cm^{-1} at 25 °C. 5mL of the electrolyte was taken in a 15ml polypropylene centrifuge tube and was then placed in a thermostatic bath. Conductivity was measured at -10, 0, 10, 25, 40 and 55 °C respectively. At each temperature step, a constant temperature was maintained for at least 2 hours to allow the electrolyte temperature to equilibrate with the bath temperature. Measurement was performed twice to confirm the reproducibility of the data.

Electrochemical full cells testing: $Na_3V_2(PO_4)_2F_3$ and HC coated on Al foil were received from TIAMAT, France. The electrodes were coated on one side of the foil with keeping the mass loading the same as commercial 18650 cells. The electrode thickness, active material to conducting carbon and binder ratio, porosity, etc. were maintained the same as in 18650 cells. Before assembling the coin cells, electrodes of 12.7mm diameter were punched and dried in a Buchi oven under vacuum (lower than 100 mbar) at 80 °C for 12 h. The electrochemical performance of NVPF/HC full cells was evaluated in 2032-type coin cells separated by two layers of glass fiber containing 150 µL of desired electrolytes. All cells were galvanostatically cycled using MPG2 potentiostat or BCS battery cycler (Bio-Logic, France), and the cycling rates were calculated with respect to NVPF (1C = 128 mA g^{-1}). For electrolyte preparation, classic organic solvents were used throughout the paper namely ethylene carbonate (EC), propylene carbonate (PC) and dimethyl carbonate (DMC) containing water amount less than 10ppm. The *Control* electrolyte throughout the paper is 1M $NaPF_6$ in EC-PC-DMC (1:1:2 by vol %). Electrolyte with Additives (or *Add*) contains 0.5% NaODFB, 3% VC, 3% SN and 0.2% TMSPi. When MA/EA is added, the mentioned x% represents that x% of solvent was replaced with MA/EA. Minimum two cells were assembled for each experiment to confirm the reproducibility of the data.

Electrochemical Impedance Spectroscopy (EIS) measurements: A BioLogic MPG2 cycler was used to measure electrochemical impedance spectra of the full coin cells. The spectra were collected over a frequency range of 20 kHz to 10 mHz with six points per decade with a perturbation amplitude of 10 mV. Spectra were collected at 10°C, 25°C, 40°C, and 55°C. Two cells were assembled for each experiment to confirm the reproducibility of the impedance data. Electrodes of 12.7mm diameter (and of 1.267 cm^2 area) were used for impedance measurements.

3. Results and Discussions

3.1 Change in bulk ionic conductivity by ester co-solvents

The *Control* or mother electrolyte for the study was taken as 1M $NaPF_6$ in EC-PC-DMC (1:1:2 by vol %). To test the change in conductivity after adding the ester co-solvents, 20% of solvent was replaced with MA or EA, and named as *20% MA + Control* and *20% EA + Control*, respectively. The bulk ionic conductivity of the *Control* electrolyte was measured as a function of temperature and is shown in Fig. 1 and the values are given in Supplementary Fig.1. A value of 11.65 mS/cm is observed at 25°C; however, it decreases to 4.75 mS/cm at -10°C. A striking increase in conductivity was observed by adding 20% MA to the *Control* electrolyte with conductivities of 13.65 mS/cm and 7.07 mS/cm at 25°C and -10°C, respectively. For the blend with EA, intermediate conductivity between MA-containing and *Control* electrolyte was observed, most likely due to the high viscosity of EA (0.46 cP at 25°C) in comparison to that of MA (0.40 cP at 25°C)[43]. Nevertheless, both MA and EA have a relatively low dielectric constant of 6.68 and 6.0, respectively[44].

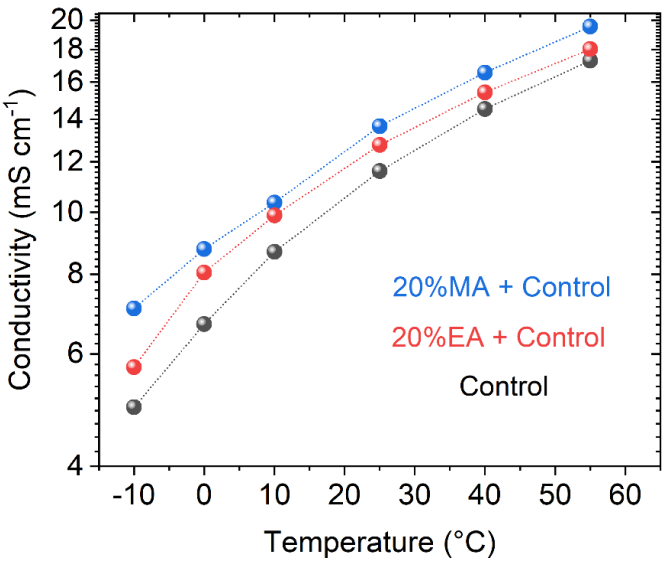

Figure 1. Ionic conductivity of the electrolyte blends *Control* (1M $NaPF_6$ in EC-PC-DMC 1:1:2 by vol %), *20%MA + Control* (1M $NaPF_6$ in EC-PC-DMC-MA 1:1:2:1 by vol %) and *20%EA + Control* (1M $NaPF_6$ in EC-PC-DMC-EA 1:1:2:1 by vol %) measured at -10°C, 0°C, 10°C, 25°C, 40°C and 55°C.

In general, cyclic carbonates (EC, PC, etc.) possess high dielectric constant and high viscosity, on the contrary linear carbonates (DMC, EMC, DEC, etc.) have low dielectric constant and low viscosity. In an ideal scenario, high ionic conductivity is observed in solvent blends having both high dielectric constant and low viscosity[45–47]. According to these observations, as the dielectric constant of the solvent blend decreases, it can create ion association, which reduces ionic conductivity. In our case, 60% of the solvent (40%DMC and 20%MA) are having the low dielectric constant, still we see increase in the ionic conductivity. It was observed by Logan et al. [48] that as low as 30%EC is sufficient for the prevention of ion association, even at high salt concentrations. In the present study, nearly 40% of cyclic carbonates (EC-PC) have been used that effectively separates the anions and cations. Hence, the bulk ionic conductivity of the electrolyte has increased significantly by the simple addition of small amount of low viscosity co-solvent (MA/EA). In summary, a noteworthy increase in ionic conductivity was observed here with the addition of MA/EA is ascribed to the low drag force experienced by ions (which were already well dissociated by EC-PC) during their migration.

3.2 Electrochemical stability of electrolyte with ester co-solvents

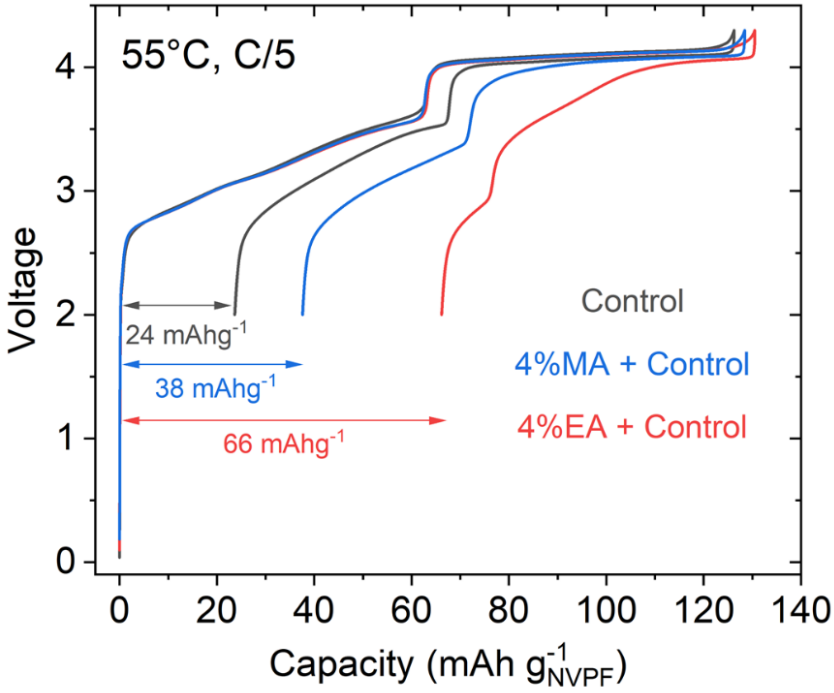

Figure 2. Voltage *vs.* Capacity profile for the first cycle of NVPF/HC coin cells using *Control*, *4%MA + Control and 4%EA + Control* electrolyte blends. The arrow in the figure represent the irreversible capacity loss in the first cycle.

The electrochemical stability of the ester co-solvent containing electrolytes was tested in Na-ion full cells having $Na_3V_2(PO_4)_2F_3$ (NVPF) and hard carbon (HC) as positive and negative electrodes (Figure 2) respectively. At first, co-solvent incorporation of as low as 4% MA/EA was tested without using any electrolyte additives. The experiments were done at high temperature (55 °C) to check for eventual degradations. The cycling curves are shown in Figure 2 together with *Control* electrolyte having no ester co-solvent. The first cycle irreversibility increases with the addition of ester co-solvent indicative of a huge Na^+ inventory loss during the formation of interphase. In addition, *4%EA+Control* has more irreversible loss than *4%MA+Control*. This finding is similar to what has been reported in the literature for LIBs with namely EA and MA having poor oxidative/reductive stabilities hence most likely the same origin for the observed irreversibility and poor cyclability of the ester containing electrolytes in NVPF-HC full cells (potential window 2- 4.3 V).

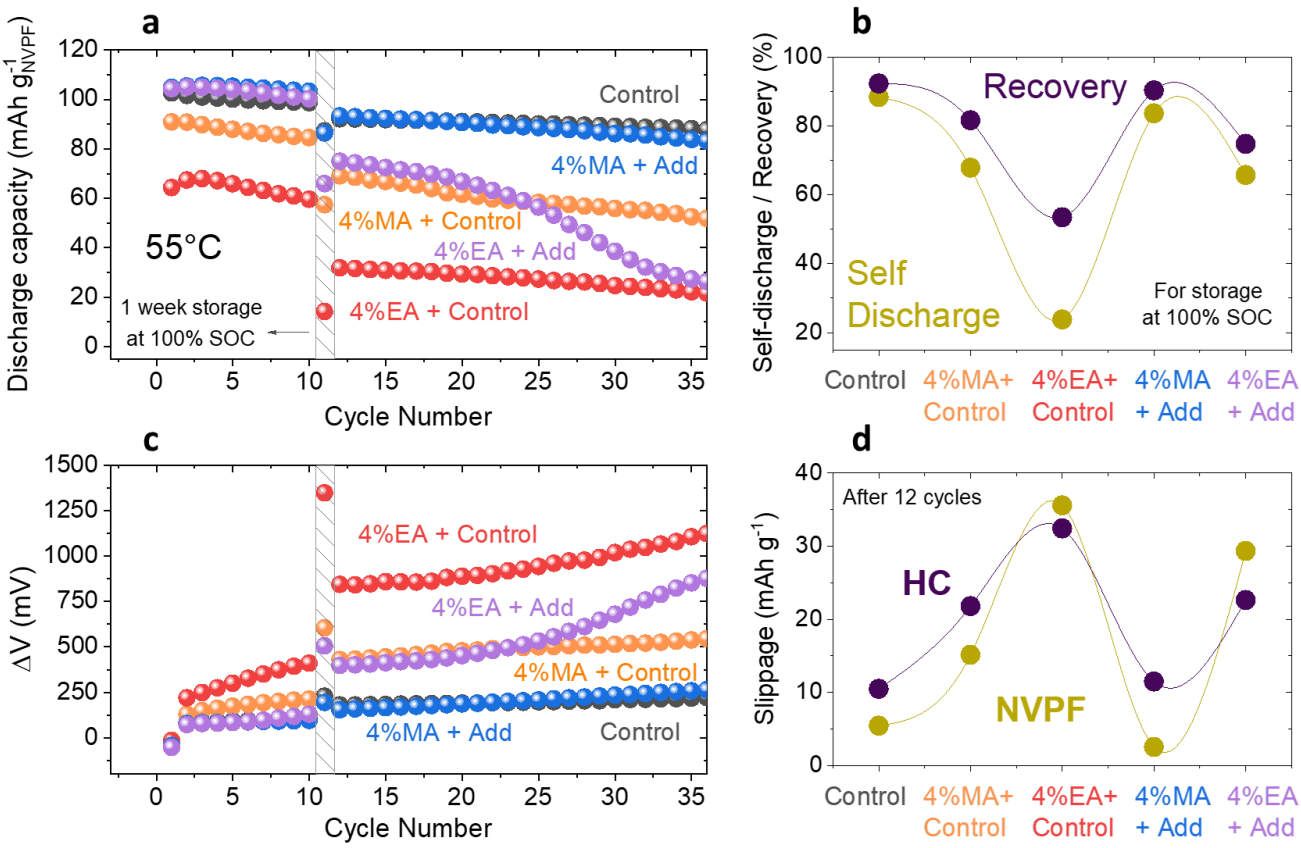

Figure 3. Electrochemical performance of NVPF/HC coin cells of five different electrolyte blends, *Control, 4%MA+Control, 4%EA+Control, 4%MA+Additives, 4%EA+Additives* cycled in 55°C oven at C/5 rate. (a) Discharge capacity (%) *vs.* cycle number for electrolytes. (b) Self-discharge (%) and recovery (%) of the cells with electrolytes during the one week storage at 100% SOC. (c) Polarization (ΔV) development as a function of cycle number for different electrolytes. (d) NVPF and HC slippage for electrolytes after 12 cycles.

In order to improve the electrochemical stability of MA/ EA containing electrolyte, the mixture of 4 additives namely, 0.5% NaODFB, 3% VC, 3% SN and 0.2% TMSPi, recently studied by our group[42] is added into the MA/ EA co-solvent containing electrolytes. The electrolyte formulations thus obtained with these additives are mentioned hereafter with the extension '*Add* ' in their name for simplicity purposes. The MA/ EA containing electrolytes formulated with or without electrolyte additives together with the *Control* (having neither MA/ EA nor additives) electrolyte were tested for their stability in *NVPF-HC* cells at *55°C*. The typical *55°C* testing protocol (explained in *Supplementary Fig.S2*) starts with 10 cycles at C/5 and then charging the cell to 4.3 V (100% SOC) and storing it for 1week at 55°C. After storage, the cells were continued to cycle and the values of self-discharge ($Q_{discharge-11}$/ $Q_{discharge-10}$ x 100) and recovery

($Q_{discharge-12}$/ $Q_{discharge-10}$ x 100) give the quantification of parasitic reactions during storage[49,50], which hamper the cell calendar life (described in *Supplementary Fig.S3)*. Further, the continuous cycling (capacity retention) gives an idea of the cell cycle life. Moreover, the polarization of the cell or ΔV is calculated as average discharge voltage subtracted from average charge voltage, which suggests impedance growth in the cell[51]. The slippage values of NVPF and HC electrodes indicate the parasitic reactions and (or) mass losses at the respective electrodes, and its calculation method is described elsewhere[42,52].

In Fig. 3a, *4%MA+Add* and *4%EA+Add* retained more capacity than 4%MA+*Control* and 4%EA+*Control*, respectively. In the presence of additives, the polarization (Fig. 3c) decreases as well as the capacity loss during self-discharge (Fig. 3b) and the slippage amplitude of NVPF and HC electrode are decreased. This indicates that additives passivate the electrodes preventing side reactions and resistance growth. Moreover, the *4%MA+Add* shows very similar behavior to that of *Control* electrolyte in terms of capacity retention, polarization, self-discharge and slippage. The MA concentration was increased up to 20% and similar stability at high temperature cycling (55 °*C*) is observed indicating the interphase stability is mainly controlled by the additives *(Supplementary Fig.S4)*. Overall, we confirmed from 55 °C testing that MA is much more stable than EA and it could be stabilized further using the additives. Hence, further studies hereafter focus solely on MA co-solvent containing 4 additives. For the sake of completion, note here that, the same 4 additives while using in electrolyte without organic esters (MA/ EA) showed much better stability at 55 °C (*supplementary Fig.S5*). We suspect such behavior can be associated with the possible degradation of MA at high temperature.

3.3 Long term cycling at ambient temperature

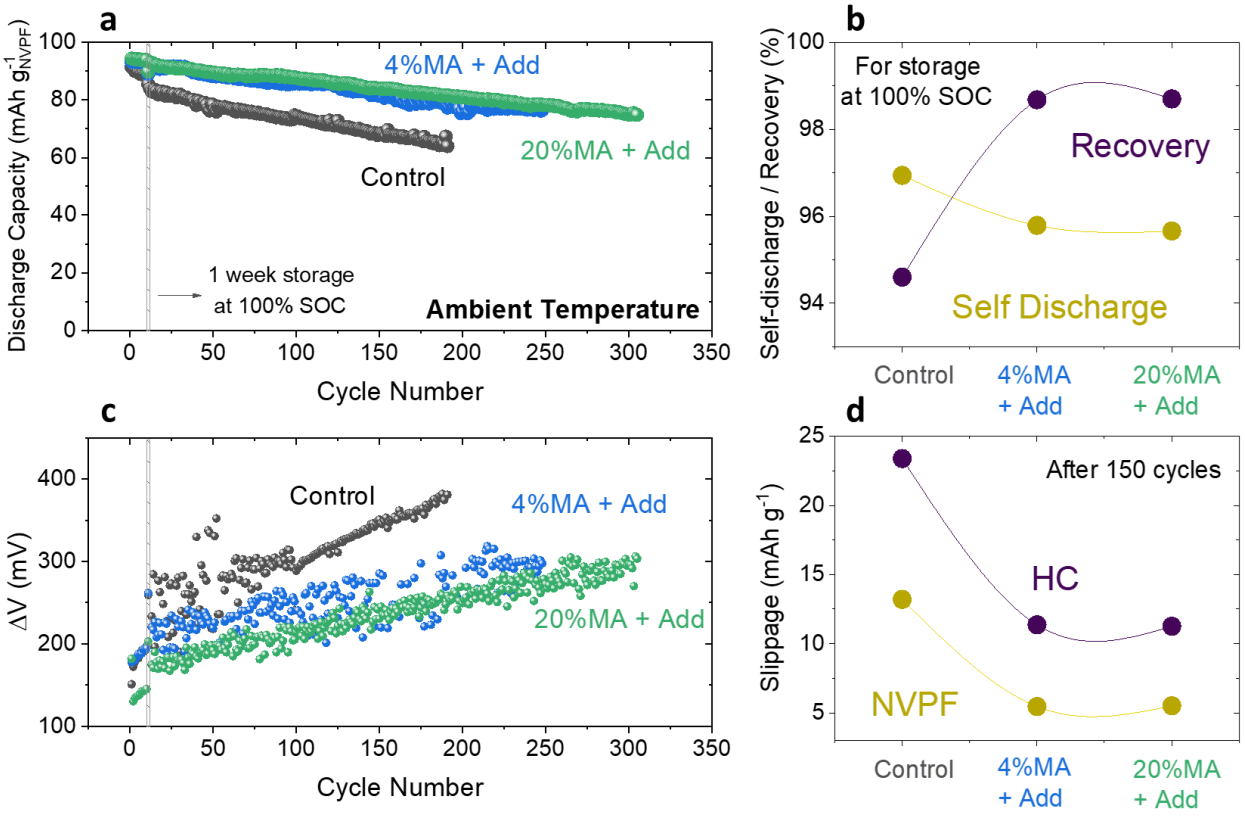

Figure 4. Electrochemical performance of NVPF/HC coin cells of three different electrolyte blends, *Control, 4%MA+Additives, 20%MA+Additives*, cycled at ambient temperature with C/5 rate. (a) Discharge capacity (%) *vs.* cycle number for electrolytes. (b) Self-discharge (%) and recovery (%) of the cells with electrolytes during the one week storage at 100% SOC. (c) Polarization (ΔV) development as a function of cycle number for different electrolytes. (d) NVPF and HC slippage for electrolytes after 150 cycles.

The long term cycling stability of the MA together with 4-additives containing electrolytes were tested at room temperature using the same protocol of cycling described in *Supplementary Fig.2*. Fig. 4a and Fig. 4c show the discharge capacity and polarization evolution with cycle for *Control*, 4%MA+*Add* and 20%MA+*Add*. All the cells containing additives show better capacity retention and less polarization than cells based on our *Control* electrolyte. After one-week of storage, recovery (Fig. 4b) was the lowest for the *Control* electrolyte while it is comparable for electrolytes with additives and different amount of MA. Slippage of NVPF and HC electrodes plotted after 150 cycles shows the same trend with more slippage for electrolyte without additives. Here, recovery (after one-week storage at 100% SOC) and slippage (calculated after 150 cycles) gives qualitative comparison of calendar life and cycle life of the cell,

respectively, with namely a similar degradation for 4% and 20% of MA. This further confirm that the additives play a major role in forming the stable interphase. At this stage, the role of additives has been mainly observed while the function of MA co-solvent is not clear. To throw some light on this issue, the cycling behavior of the MA containing electrolytes were tested at low temperature to enhance the effect of electrolyte resistance.

3.4 Electrochemical behavior of MA containing electrolytes for low temperature applications

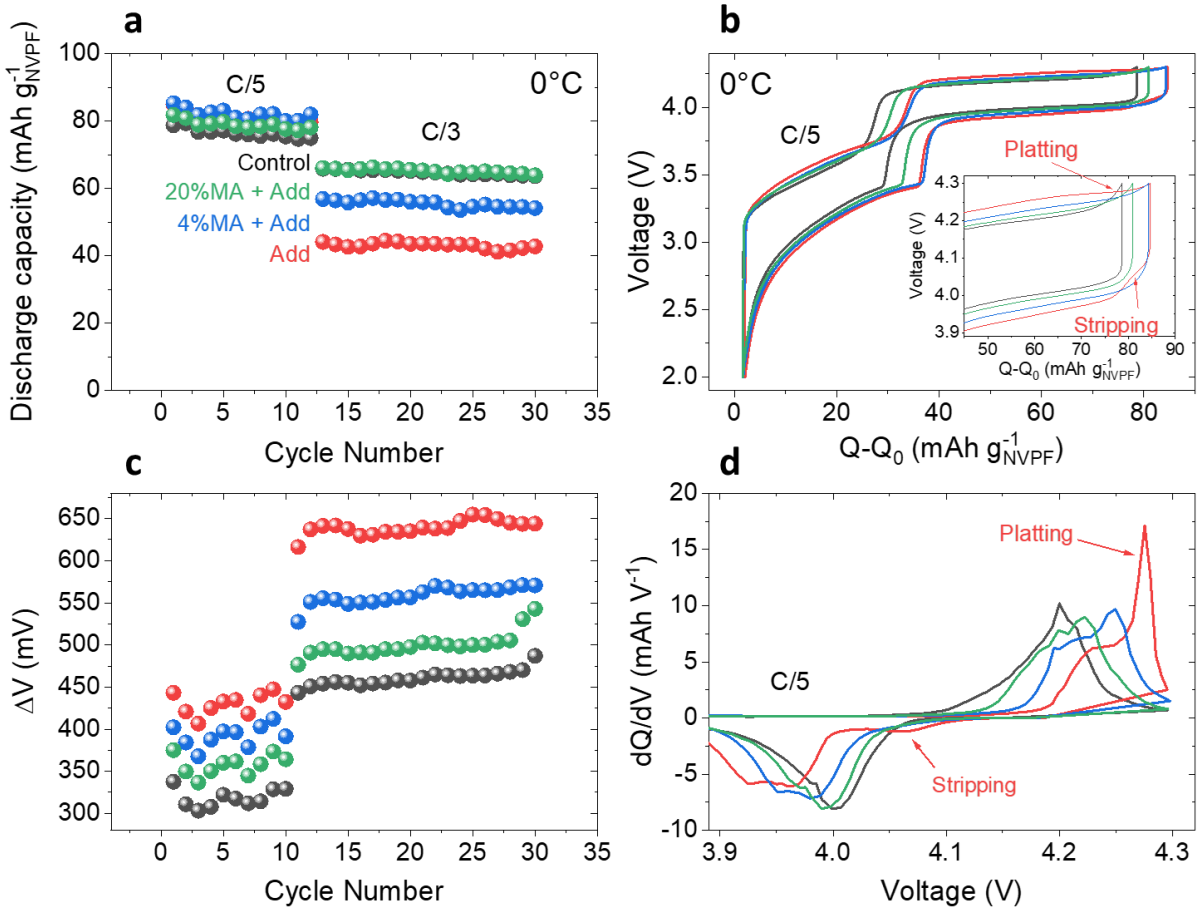

Figure 5. Electrochemical performance of NVPF/HC coin cells of four different electrolyte blends, *Control*, *Additives*, *4%MA+Additives*, *20%MA+Additives*, cycled at 0°C with C/5 and C/3 rate. (a) Discharge capacity (%) *vs.* cycle number for electrolytes. (b) Voltage *vs.* Q-Q_0 profile of the second cycle. (c) Polarization (ΔV) as a function of cycle number for different electrolytes. (d) dQ/dV *vs.* V of the second cycle represented in (b)

Fig. 5a and Fig. 5c show the discharge capacity and polarization evolution for cells with *Control*, *Add* (with additives and no ester co-solvent), *4%MA+Add* and *20%MA+Add* electrolyte at 0°C. At a C/5 rate, the capacity of all the cells is comparable but polarization trend differs as "*Add* > *4%MA+Add* > *20%MA+Add* > *Control*". The charging profile of the cells is shown in Fig.5b. The cell with *Add* (red curve) in the inset of Fig. 5b shows signs of sodium platting during charge and stripping during discharge. More evidently, the dQ/dV of the charging profiles presented in Fig. 5d shows a clear signature of sodium plating and stripping. When the rate increased to C/3, the trend for polarization (Fig. 5c) is same with higher magnitude. Still the cells having more polarization resulted in less capacity due to an early hitting of the cut-off voltage and the trend of capacity changed to "*Control ~ 20%MA+Add* > *4%MA+Add* > *Add*". In this scenario, the 20%MA was very efficient in reducing the polarization and consequently achieving higher capacity at C/3 with no sign of sodium platting than the cells with only *Additives (Add)*. Previously, in Li-ion batteries, it was claimed that high conductivity coming from MA reduces the concentration polarization at the negative electrode interphase and by the same token reduces the chances of metal plating. To check whether the same is true with NVPF-HC sodium-ion cells, we studied next the impedance behavior of the cells containing different electrolyte formulations, with or without MA co-solvent.

3.5 Charge transfer resistance identification

A difficulty here resides in the correct identification of the resistances associated with ionic/electronic transports, cell components and interfaces of the electrodes/current collectors from the charge transfer resistance. To overcome this difficulty, we used the strategy of blocking and non-blocking electrodes state reported elsewhere[53]. During PEIS, in the blocking state, there is no sodium insertion/extraction from the electrodes[54] but there is sodium migration in the electrolyte due to voltage pulse. Conversely, in non-blocking state there is sodium insertion/extraction in addition to sodium migration in the electrolyte. Here, the blocking state is identified as 0 % SOC and for convenience, non-blocking state is taken as 100% SOC. Fig. 6a shows the impedance plot of the NVPF-HC cells in blocking and non-blocking state at 25 °C. Cells in blocking state show only one semi-circle at high frequency but non-blocking state

shows two semi-circles at both high and low frequency. A similar nature of impedance spectra was observed in case of lithium-ion cells[53].Thus, the low frequency semi-circle in non-blocking state corresponds to only the charge transfer and the high frequency semicircle corresponds to all the other resistances. Interestingly, when temperature is lowered to 0 °C (Fig.6b), the relation between blocking and non-blocking state remains the same but there is huge increase in the charge transfer semicircle and very slight increase in the other resistances. This indicates that at low temperature, charge transfer impedance contributes to the majority of cell impedance. The impedance model and details of corresponding resistances are given in Supplementary Fig. S6. R_S (solution resistance) cumulates the electrode electronic resistance and the electrolyte ionic resistance. On the other hand $R_{contact}$ encompasses all the coin cell contacts and the CPE parallel to it represents constant phase element (from imperfect capacitive effects) from all the interfaces like electrode film and current collector etc. Lastly, the desolvation of Na^+, its travel across interphase and into the electrode particle is denoted as $R_{charge\ transfer}$ and the CPE parallel to it is from the double layer capacitance at the electrode interface.

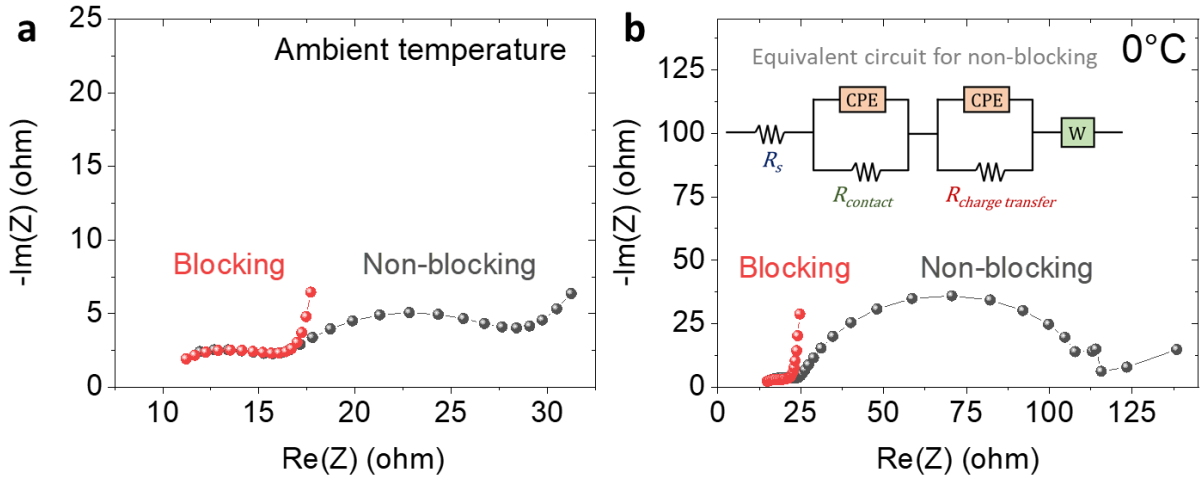

Figure 6. Electrochemical impedance spectroscopy in blocking and non-blocking configuration of the NVPF/HC cells containing electrolyte with additives at (a) ambient temperature and (b) 0°C with equivalent circuit model for non-blocking configuration. The scale of X and Y-axis are in 1:1 ratio and electrode area is 1.267 cm^2.

Now, to compare the charge transfer resistance, four electrolytes, namely *Control, Add, 4%MA+Add, 20%MA+Add* are used. The protocol used for impedance

includes two cycles at 55 °C, 40 °C, 25 °C, 10 °C respectively and PEIS at 100% SOC during those cycles. Fig.7 shows the impedance curves at various temperatures for different electrolytes. It is important to note that we start to see the charge transfer resistance only at the 25°C, thus for our system, at temperatures higher than 25°C it is challenging to fit and get reliable charge transfer resistance value. The impedance curve of electrolytes at 25°C and 10°C was fitted and the values of R_s (solution resistance), $R_{contact}$ (contact resistance) and $R_{charge\ transfer}$ (charge transfer resistance) are given in Supplementary Fig.S7.

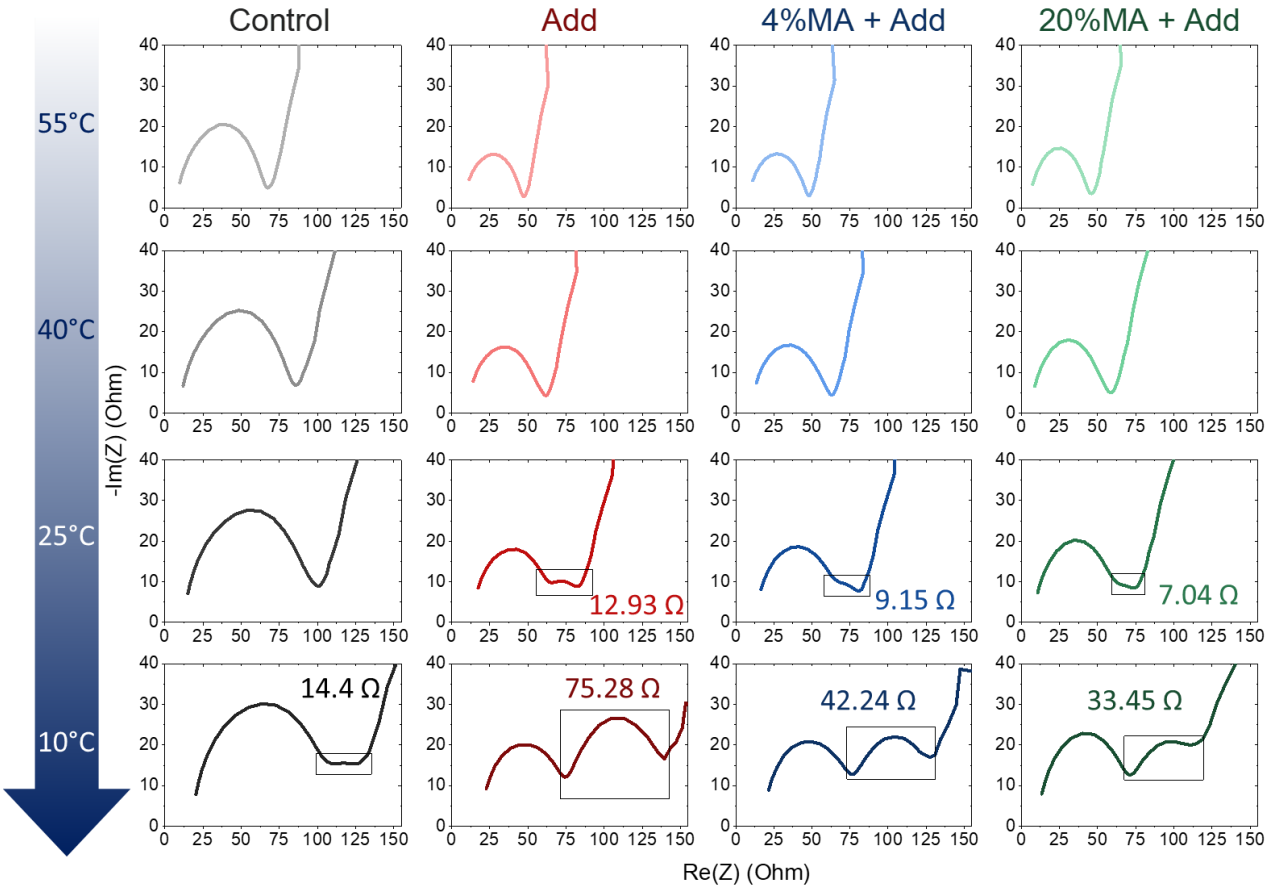

Figure 7. Electrochemical impedance spectroscopy in non-blocking configuration and 100% SOC of the NVPF/HC cells containing four different electrolytes, namely *Control, Additives, 4%MA+Additives, 20%MA+Additives* at 55°C, 40°C, 25°C and 10°C. Scale of X and Y-axis are not in 1:1 ratio and electrode area is 1.267 cm^2

Charge transfer resistance in Fig.7 at 10°C was the lowest for *Control* (14.4 Ω) and highest for electrolyte having 4-additives with no co-solvent (*Add,* 75.28 Ω). With

the addition of MA co-solvent, the charge transfer decreased, for 4%MA+Add it was 42.24 Ω and 20%MA+Add was 33.45 Ω. Two possible reasons could account for the decrease in charge transfer with MA. Firstly, with MA the ionic conductivity was increased and during the voltage pulse of PEIS there will be less depletion of sodium ions from electrode interphases because of the fast sodium migration in electrolytes with MA as compared to electrolyte without MA. Secondly, MA could participate to the primary/secondary solvation sheath of sodium and this is changing the (de)solvation energy during insertion/extraction. Both of these phenomena are complicated and intertwined thus it is difficult to differentiate which of them is affecting the charge transfer, and to what extent.

Conclusively, it seems here that *Control* electrolyte is the best choice for high power and low temperature commercial applications. However, the total cell resistance ($R_{charge\ transfer}$ + $R_{contact}$) for temperatures equal to or higher than the 25°C is largest for the *Control* electrolyte (Fig.7). Additionally, the stability of the electrolyte at ambient temperatures is the least for *Control* electrolyte (Fig. 4a). Finally, it was convenient to use additives that will increase the cell lifetime at ambient/high temperatures and reduce the impedance at low temperatures as done in the case of MA co-solvent. On this note, next we try to check the effect of MA on the power performance of commercial NVPF-HC cells containing additives.

3.6 Power performance and high temperature stability in 18650 cells

In short, MA co-solvent reduces the charge transfer resistance and increases the ionic conductivity hence supporting the better Na-ion conduction at low temperatures. However, the improvement in electrolyte conductivity does not significantly influence room/ high temperature applications when the cells were cycled at slower C/5 rates (Figure 2-4). Hence, next we studied the cycling performance of the MA containing electrolytes by increasing the charge/discharge cycling rates. Towards this purpose, we filled NVPF-HC based dry 18650 cells from TIAMAT Energy with either *control* (with no additives) or *20% MA+ Add* electrolyte. The cells were formatted using the TIAMAT formation protocol and impedance analyses, once the cell formation achieved, were carried out at 25°C at 100% SOC (Fig. 8a) as well as at 50 % SOC (supplementary Fig.

S8). Comparatively lower impedance was observed for *20% MA+ Add* electrolyte containing cells in both SOC. This supports the impedance experiments performed in coin cells at 25°C and 4.3V since the lowest cumulated $R_{charge\ transfer}$ + $R_{contact}$ resistance was observed for *20%MA + Add* electrolyte (cf. Fig.7). Fig. 8b compares the initial cycles at C/5 where the 1C or 1D defined in reference to a reversible capacity of ~105 mAh/g of NVPF (720 mAh in the used 18650 cell design). The *20% MA+ Add* shows higher reversible capacity than the *control* indicating larger electrolyte decomposition during formation cycles. It should be noted here that, though the full capacity is observed with *20% MA+ Add electrolyte*, the cycling profile shows an average polarization of ~85 mV with the higher voltage gap observed in the low voltage region (<3.6 V) than the high voltage one (>3.6 V). Such polarization is mainly associated with the electrode materials as both NVPF and HC exhibits voltage hysteresis [55,56] of thermodynamic nature (e.g zero-current voltage gap; see Supplementary Fig. S9 for more details)) with the one for HC being the larger in the low voltage regions. Upon increasing the cycling rates, the voltage gap between charge and discharge increases (inset of Fig. 8c) and reaches a maximum of ~270 mV at 5C rate for both *control* as well as *20% MA+ Add* electrolytes. The cycling profile in Fig. 8c shows nearly similar polarization for both, with however a less capacity for the *control* electrolyte, which could be because of the initial poor capacity after the formation.

The capacity retention at each rate for *control* as well as *20% MA+ Add* electrolytes are cumulated in Fig. 8d and 8e respectively, with the percentage capacity retention (charge) plot in Fig. 8f. A slow rate (C/5: D/5) cycling is carried out every fifth cycle (before moving from one rate test to another) in order to reduce the possible heat formed during fast charge-discharge cycles. Further, when going from C/5 to 3C, the capacity difference observed between *control* and *20% MA+ Add* electrolytes is large. However, the change in capacity is almost negligible on moving from 3C to 4C or 5C (Fig. 8f). As a result, nearly 79% capacity is retained at 5C for *control* and a maximum of 84% is retained for *20% MA+ Add*. This is counter intuitive and we do not yet have an explanation to account for this finding.

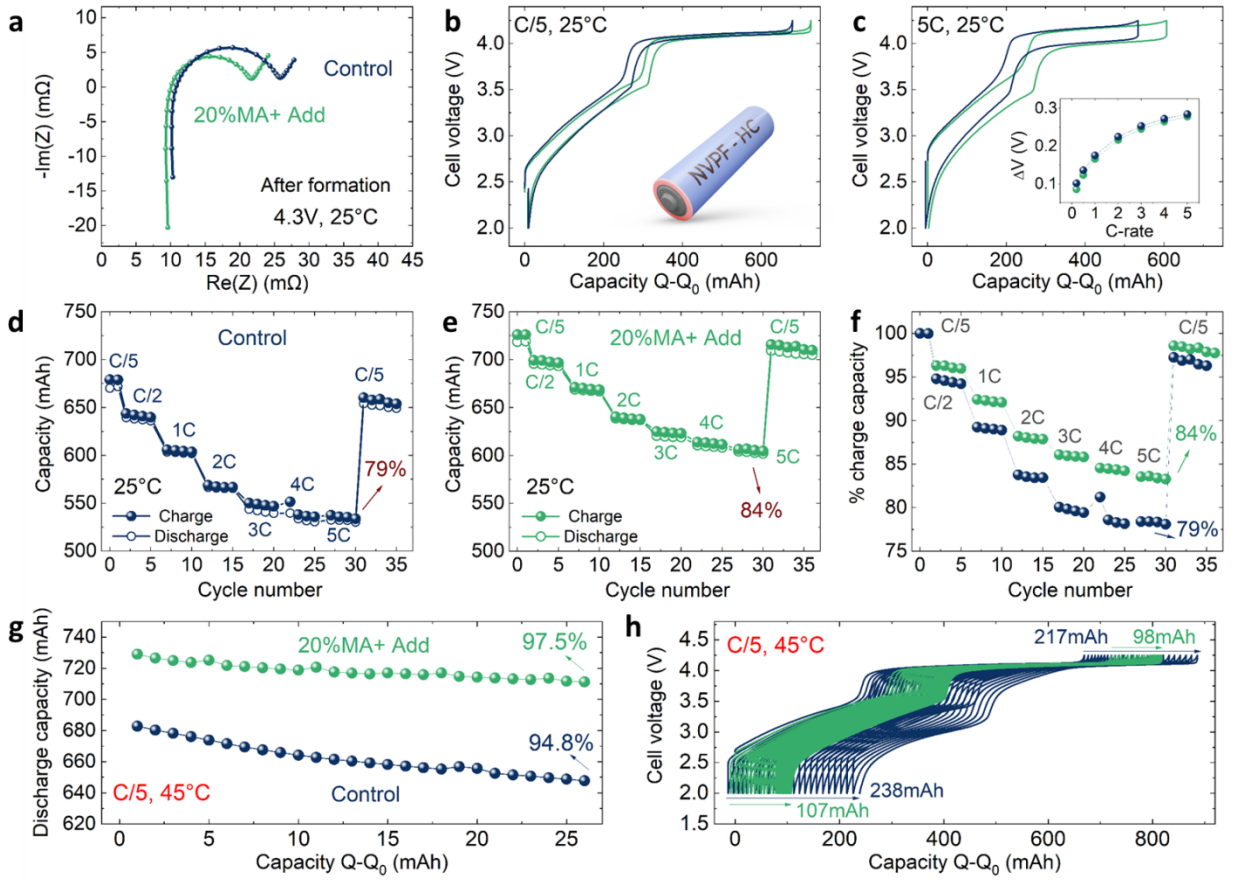

Figure 8. The electrochemical performance of cylindrical 18650 NVPF/HC cells filled with *Control* or *20%MA+Add* electrolytes (a) Impedance spectra taken at 100% SOC or 4.3V of the cell at 25 °C. (b) Charge profiles at C/5 and 25 °C. (c) Charge profiles at 5C and 25 °C with inset containing cell's average polarization at different rates. (d) Rate behavior of the *Control* electrolyte in absolute capacity *vs.* cycle number (e) Rate behavior of the *20%MA+Add* electrolyte in absolute capacity *vs.* cycle number (f) Rate comparison of *Control and 20%MA+Add* electrolytes in terms of charge capacity(%) *vs.* cycle number. (g) Capacity retention of the cells containing *Control and 20%MA+Add* electrolytes at 45 °C with the (f) corresponding cycling profiles for 1- 25 cycles.

Overall, both *control* and *20% MA+ Add* electrolyte exhibit excellent rate capabilities close to 80% while charging the cell as fast as 10 min (5C). The added advantage with *20% MA+ Add* comes from its cycling stability as ~98% of its initial capacity is retained on moving back to C/5 after all the rate capability tests while the *Control* electrolyte recovered only 96% of its initial capacity on moving back to C/5. Moreover, upon additional cycling at high temperature (45 °C; Fig. 8g), we note a better stability of 97.5% with *20% MA+ Add* than the *Control* electrolyte (94.8% retention) after 25 cycles. The cycling profile of the cells at 45°C (Fig. 8h) also indicates reduced charge/ discharge endpoint slippage for *20% MA+ Add* (charge endpoint slippage: 98

mAh; discharge endpoint slippage 107mAh) in comparison to *Control* (charge endpoint slippage: 217 mAh; discharge endpoint slippage 238mAh). Such difference in charge/ discharge endpoint slippage also hints towards less parasitic reactions and better interphase stability of *20% MA+ Add* electrolyte indicating better cycle life at high temperature. The Long cycling performance at 25° C of fresh 18650 cell using *20% MA+ Add* electrolyte, confirm the ambient temperature stability as mentioned in Supplementary Fig. S10.

	Low Temperatures (<10°C)			Medium Temperatures (~25°C)			High Temperatures (>45°C)		
	Control	*Add*	*MA + Add*	*Control*	*Add*	*MA + Add*	*Control*	*Add*	*MA + Add*
Ionic conductivity	😐	😐	🙂	😐	😐	🙂	🙂	🙂	🙂
Cycle life	🙂	☹	🙂	☹	🙂	🙂	😐	🙂	😐
Calendar life	-	-	-	☹	🙂	🙂	😐	🙂	😐
Plating related Na^+-loss	🙂	☹	🙂	-	-	-	-	-	-
Impedance (R_{ct} + $R_{contact}$)	🙂	☹	🙂	☹	😐	🙂	😐	🙂	🙂
Power	-	-	-	🙂	😐	🙂	-	-	-

Degree of appropriateness: 🙂, good; 😐, average; ☹, bad.

Figure 9. Summary of the relative comparison of the different observables that are the key for evaluating battery performance and safety. *Control* is the mother electrolyte, *Add* is the electrolyte containing additives and *MA+Add* is the electrolyte containing both additives as well as MA co-solvent.

The various test parameters studied till now were cumulated together in table (in Fig. 9). The electrolyte properties at different temperatures were compared for three different electrolytes namely, *Control*, with additives (*Add*) and with additives and MA co-solvent (*MA+ Add*). Among the three, the *Control* electrolyte with poor cycling stability at medium/ high temperature is least favored though it exhibit high power performance and low temperature applications. In contrary, the electrolyte '*Add*' exhibit high cycling stability at medium/ high temperature and suits well for high temperature applications. However, the power performance and low temperature applications are limited mainly due to the interphase resistance. Now, the MA co-solvent added electrolyte exhibit intermediate properties with good low temperature performance,

comparatively better power performance and cycling stability. It shows the suitability of MA co-solvent for improved power and low temperature applications. However, one has to remember that the high temperature performance is relatively compromised with MA co-solvent and the electrolyte need to be selected based on the application requirement. Overall, extraordinary charging capability of 84% at 5C (charged in 10-11 min) together with the improved cycling stability observed with *20% MA+ Add* is very encouraging and is very close to meet the “extreme fast charging” (XFC) goal of the automotive market[57]. For a perspective, further improvement in power performance of the MA+ Add electrolyte can be achieved by optimizing the electrolyte additives to form low resistive/ highly stable interphases. The efforts are ongoing to find suitable co-additives, which will decrease the low/medium temperature impedance without affecting high temperature stability. By combining such electrolyte additives in parallel with the incorporation of MA co-solvent, the aim is to reach 80% capacity in 5min charging time together with long cycle life without compromising the safety of the cells.

Acknowledgements:

The authors thank the RS2E Network for funding as well as the financial support of Région Nouvelle Aquitaine, of the French National Research Agency (STORE-EX Labex Project ANR-10-LABX-76-01). S. M, J. A-R and J.-M. T acknowledges the funding from the project NAIMA (Horizon 2020 research and innovation program under grant agreement No 875629). P. D thanks RS2E for PhD funding. We thank Quentin LOISELEUX from TIAMAT, France for providing the NVPF/HC 18650 cells as well as the NVPF, HC electrodes for the study.

References

[1] B. Dunn, H. Kamath, J.-M. Tarascon, Electrical Energy Storage for the Grid: A Battery of Choices, Science. (2011). https://doi.org/10.1126/science.1212741.

[2] Z.P. Cano, D. Banham, S. Ye, A. Hintennach, J. Lu, M. Fowler, Z. Chen, Batteries and fuel cells for emerging electric vehicle markets, Nat Energy. 3 (2018) 279–289. https://doi.org/10.1038/s41560-018-0108-1.

[3] Y. Liu, R. Zhang, J. Wang, Y. Wang, Current and future lithium-ion battery manufacturing, IScience. 24 (2021) 102332. https://doi.org/10.1016/j.isci.2021.102332.

[4] M. Weil, S. Ziemann, J. Peters, The Issue of Metal Resources in Li-Ion Batteries for Electric Vehicles, in: G. Pistoia, B. Liaw (Eds.), Behaviour of Lithium-Ion Batteries in Electric Vehicles: Battery Health,

Performance, Safety, and Cost, Springer International Publishing, Cham, 2018: pp. 59–74. https://doi.org/10.1007/978-3-319-69950-9_3.
[5] G. Crabtree, The coming electric vehicle transformation, Science. (2019). https://doi.org/10.1126/science.aax0704.
[6] E.A. Olivetti, G. Ceder, G.G. Gaustad, X. Fu, Lithium-Ion Battery Supply Chain Considerations: Analysis of Potential Bottlenecks in Critical Metals, Joule. 1 (2017) 229–243. https://doi.org/10.1016/j.joule.2017.08.019.
[7] Lithium hexafluorophosphate (LiPF6) price continues to rise-China market news, (n.d.). http://www.cnchemicals.com/Press/91601-Lithium%20hexafluorophosphate%20(LiPF6)%20price%20continues%20to%20rise.html (accessed January 9, 2022).
[8] Lithium carbonate prices break through $40/kg barrier, Benchmark Mineral Intelligence. (n.d.). https://www.benchmarkminerals.com/membership/lithium-carbonate-prices-break-through-40-kg-barrier/ (accessed January 9, 2022).
[9] Y. Tian, G. Zeng, A. Rutt, T. Shi, H. Kim, J. Wang, J. Koettgen, Y. Sun, B. Ouyang, T. Chen, Z. Lun, Z. Rong, K. Persson, G. Ceder, Promises and Challenges of Next-Generation "Beyond Li-ion" Batteries for Electric Vehicles and Grid Decarbonization, Chem. Rev. 121 (2021) 1623–1669. https://doi.org/10.1021/acs.chemrev.0c00767.
[10] C. Vaalma, D. Buchholz, M. Weil, S. Passerini, A cost and resource analysis of sodium-ion batteries, Nat Rev Mater. 3 (2018) 18013. https://doi.org/10.1038/natrevmats.2018.13.
[11] Department of Energy Announces $19 Million for Advanced Battery and Electrification Research to Enable Extreme Fast Charging, Energy.Gov. (n.d.). https://www.energy.gov/articles/department-energy-announces-19-million-advanced-battery-and-electrification-research-enable (accessed January 10, 2022).
[12] J.-M. Tarascon, Na-ion versus Li-ion Batteries: Complementarity Rather than Competitiveness, Joule. 4 (2020) 1616–1620. https://doi.org/10.1016/j.joule.2020.06.003.
[13] T. Broux, F. Fauth, N. Hall, Y. Chatillon, M. Bianchini, T. Bamine, J.-B. Leriche, E. Suard, D. Carlier, Y. Reynier, L. Simonin, C. Masquelier, L. Croguennec, High Rate Performance for Carbon-Coated Na3V2(PO4)2F3 in Na-Ion Batteries, Small Methods. 3 (2019) 1800215. https://doi.org/10.1002/smtd.201800215.
[14] R. Usiskin, Y. Lu, J. Popovic, M. Law, P. Balaya, Y.-S. Hu, J. Maier, Fundamentals, status and promise of sodium-based batteries, Nat Rev Mater. 6 (2021) 1020–1035. https://doi.org/10.1038/s41578-021-00324-w.
[15] D.A. Stevens, J.R. Dahn, High Capacity Anode Materials for Rechargeable Sodium-Ion Batteries, J. Electrochem. Soc. 147 (2000) 1271. https://doi.org/10.1149/1.1393348.
[16] A. Nyman, T.G. Zavalis, R. Elger, M. Behm, G. Lindbergh, Analysis of the Polarization in a Li-Ion Battery Cell by Numerical Simulations, J. Electrochem. Soc. 157 (2010) A1236. https://doi.org/10.1149/1.3486161.
[17] Y. Liu, Y. Zhu, Y. Cui, Challenges and opportunities towards fast-charging battery materials, Nat Energy. 4 (2019) 540–550. https://doi.org/10.1038/s41560-019-0405-3.
[18] S.S. Zhang, Unveiling Capacity Degradation Mechanism of Li-ion Battery in Fast-charging Process, ChemElectroChem. 7 (2020) 555–560. https://doi.org/10.1002/celc.201902050.
[19] S. Schindler, M. Bauer, H. Cheetamun, M.A. Danzer, Fast charging of lithium-ion cells: Identification of aging-minimal current profiles using a design of experiment approach and a mechanistic degradation analysis, Journal of Energy Storage. 19 (2018) 364–378. https://doi.org/10.1016/j.est.2018.08.002.

[20] Q. Liu, C. Du, B. Shen, P. Zuo, X. Cheng, Y. Ma, G. Yin, Y. Gao, Understanding undesirable anode lithium plating issues in lithium-ion batteries, RSC Advances. 6 (2016) 88683–88700. https://doi.org/10.1039/C6RA19482F.
[21] M. Petzl, M. Kasper, M.A. Danzer, Lithium plating in a commercial lithium-ion battery – A low-temperature aging study, Journal of Power Sources. 275 (2015) 799–807. https://doi.org/10.1016/j.jpowsour.2014.11.065.
[22] X. Lin, K. Khosravinia, X. Hu, J. Li, W. Lu, Lithium Plating Mechanism, Detection, and Mitigation in Lithium-Ion Batteries, Progress in Energy and Combustion Science. 87 (2021) 100953. https://doi.org/10.1016/j.pecs.2021.100953.
[23] J. Landesfeind, T. Hosaka, M. Graf, K. Kubota, S. Komaba, H.A. Gasteiger, Comparison of Ionic Transport Properties of Non-Aqueous Lithium and Sodium Hexafluorophosphate Electrolytes, J. Electrochem. Soc. 168 (2021) 040538. https://doi.org/10.1149/1945-7111/abf8d9.
[24] G. Yan, D. Alves-Dalla-Corte, W. Yin, N. Madern, G. Gachot, J.-M. Tarascon, Assessment of the Electrochemical Stability of Carbonate-Based Electrolytes in Na-Ion Batteries, J. Electrochem. Soc. 165 (2018) A1222–A1230. https://doi.org/10.1149/2.0311807jes.
[25] H. Hijazi, P. Desai, S. Mariyappan, Non-Aqueous Electrolytes for Sodium-Ion Batteries: Challenges and Prospects Towards Commercialization, Batteries & Supercaps. 4 (2021) 881–896. https://doi.org/10.1002/batt.202000277.
[26] A. Tomaszewska, Z. Chu, X. Feng, S. O'Kane, X. Liu, J. Chen, C. Ji, E. Endler, R. Li, L. Liu, Y. Li, S. Zheng, S. Vetterlein, M. Gao, J. Du, M. Parkes, M. Ouyang, M. Marinescu, G. Offer, B. Wu, Lithium-ion battery fast charging: A review, ETransportation. 1 (2019) 100011. https://doi.org/10.1016/j.etran.2019.100011.
[27] M. Weiss, R. Ruess, J. Kasnatscheew, Y. Levartovsky, N.R. Levy, P. Minnmann, L. Stolz, T. Waldmann, M. Wohlfahrt-Mehrens, D. Aurbach, M. Winter, Y. Ein-Eli, J. Janek, Fast Charging of Lithium-Ion Batteries: A Review of Materials Aspects, Advanced Energy Materials. 11 (2021) 2101126. https://doi.org/10.1002/aenm.202101126.
[28] S.S. Zhang, L. Ma, J.L. Allen, J.A. Read, Stabilizing Capacity Retention of Li-Ion Battery in Fast-Charge by Reducing Particle Size of Graphite, J. Electrochem. Soc. 168 (2021) 040519. https://doi.org/10.1149/1945-7111/abf40c.
[29] Y. Zhang, J.A. Alarco, J.Y. Nerkar, A.S. Best, G.A. Snook, P.C. Talbot, Improving the Rate Capability of LiFePO4 Electrode by Controlling Particle Size Distribution, J. Electrochem. Soc. 166 (2019) A4128. https://doi.org/10.1149/2.0621916jes.
[30] Z. Du, D.L. Wood, I. Belharouak, Enabling fast charging of high energy density Li-ion cells with high lithium ion transport electrolytes, Electrochemistry Communications. 103 (2019) 109–113. https://doi.org/10.1016/j.elecom.2019.04.013.
[31] J. Zheng, M.H. Engelhard, D. Mei, S. Jiao, B.J. Polzin, J.-G. Zhang, W. Xu, Electrolyte additive enabled fast charging and stable cycling lithium metal batteries, Nat Energy. 2 (2017) 1–8. https://doi.org/10.1038/nenergy.2017.12.
[32] E.J. Plichta, S. Slane, Conductivity of lithium imide in mixed aprotic solvents for lithium cells, Journal of Power Sources. 69 (1997) 41–45. https://doi.org/10.1016/S0378-7753(97)02545-7.
[33] D.E. Irish, Z. Deng, M. Odziemkowski, Raman spectroscopic and electrochemical studies of lithium battery components, Journal of Power Sources. 54 (1995) 28–33. https://doi.org/10.1016/0378-7753(94)02035-2.
[34] M.C. Smart, B.V. Ratnakumar, S. Surampudi, Y. Wang, X. Zhang, S.G. Greenbaum, A. Hightower, C.C. Ahn, B. Fultz, Irreversible Capacities of Graphite in Low-Temperature Electrolytes for Lithium-Ion Batteries, J. Electrochem. Soc. 146 (1999) 3963. https://doi.org/10.1149/1.1392577.

[35] M.C. Smart, B.V. Ratnakumar, S. Surampudi, Use of Organic Esters as Co-solvents in Electrolytes for Lithium-Ion Batteries with Improved Low Temperature Performance, J. Electrochem. Soc. 149 (2002) A361. https://doi.org/10.1149/1.1453407.
[36] X. Ma, J. Li, S.L. Glazier, L. Ma, K.L. Gering, J.R. Dahn, A study of highly conductive ester co-solvents in Li[Ni0.5Mn0.3Co0.2]O2/Graphite pouch cells, Electrochimica Acta. 270 (2018) 215–223. https://doi.org/10.1016/j.electacta.2018.03.006.
[37] D.S. Hall, A. Eldesoky, E.R. Logan, E.M. Tonita, X. Ma, J.R. Dahn, Exploring Classes of Co-Solvents for Fast-Charging Lithium-Ion Cells, J. Electrochem. Soc. 165 (2018) A2365–A2373. https://doi.org/10.1149/2.1351810jes.
[38] J. Li, H. Li, X. Ma, W. Stone, S. Glazier, E. Logan, E.M. Tonita, K.L. Gering, J.R. Dahn, Methyl Acetate as a Co-Solvent in NMC532/Graphite Cells, J. Electrochem. Soc. 165 (2018) A1027–A1037. https://doi.org/10.1149/2.0861805jes.
[39] J. Marcicki, A.T. Conlisk, G. Rizzoni, A lithium-ion battery model including electrical double layer effects, Journal of Power Sources. 251 (2014) 157–169. https://doi.org/10.1016/j.jpowsour.2013.11.001.
[40] J.-N. Chazalviel, Electrochemical aspects of the generation of ramified metallic electrodeposits, Phys. Rev. A. 42 (1990) 7355–7367. https://doi.org/10.1103/PhysRevA.42.7355.
[41] M.Z. Mayers, J.W. Kaminski, T.F. Miller, Suppression of Dendrite Formation via Pulse Charging in Rechargeable Lithium Metal Batteries, J. Phys. Chem. C. 116 (2012) 26214–26221. https://doi.org/10.1021/jp309321w.
[42] P. Desai, J. Huang, H. Hijazi, L. Zhang, S. Mariyappan, J. Tarascon, Deciphering Interfacial Reactions via Optical Sensing to Tune the Interphase Chemistry for Optimized Na-Ion Electrolyte Formulation, Adv. Energy Mater. (2021) 2101490. https://doi.org/10.1002/aenm.202101490.
[43] E.R. Logan, E.M. Tonita, K.L. Gering, J. Li, X. Ma, L.Y. Beaulieu, J.R. Dahn, A Study of the Physical Properties of Li-Ion Battery Electrolytes Containing Esters, J. Electrochem. Soc. 165 (2018) A21. https://doi.org/10.1149/2.0271802jes.
[44] A. Jänes, E. Lust, Use of organic esters as co-solvents for electrical double layer capacitors with low temperature performance, Journal of Electroanalytical Chemistry. 588 (2006) 285–295. https://doi.org/10.1016/j.jelechem.2006.01.003.
[45] Y. Matsuda, H. Satake, Mixed Electrolyte Solutions of Propylene Carbonate and Dimethoxyethane for High Energy Density Batteries, J. Electrochem. Soc. 127 (1980) 877. https://doi.org/10.1149/1.2129774.
[46] Y. Matsuda, M. Morita, K. Kosaka, Conductivity of the Mixed Organic Electrolyte Containing Propylene Carbonate and 1,2-Dimethoxyethane, J. Electrochem. Soc. 130 (1983) 101. https://doi.org/10.1149/1.2119630.
[47] K. Xu, Nonaqueous Liquid Electrolytes for Lithium-Based Rechargeable Batteries, Chem. Rev. 104 (2004) 4303–4418. https://doi.org/10.1021/cr030203g.
[48] E.R. Logan, E.M. Tonita, K.L. Gering, L. Ma, M.K.G. Bauer, J. Li, L.Y. Beaulieu, J.R. Dahn, A Study of the Transport Properties of Ethylene Carbonate-Free Li Electrolytes, J. Electrochem. Soc. 165 (2018) A705. https://doi.org/10.1149/2.0981803jes.
[49] G. Yan, K. Reeves, D. Foix, Z. Li, C. Cometto, S. Mariyappan, M. Salanne, J. Tarascon, A New Electrolyte Formulation for Securing High Temperature Cycling and Storage Performances of Na-Ion Batteries, Adv. Energy Mater. 9 (2019) 1901431. https://doi.org/10.1002/aenm.201901431.
[50] C. Cometto, G. Yan, S. Mariyappan, J.-M. Tarascon, Means of Using Cyclic Voltammetry to Rapidly Design a Stable DMC-Based Electrolyte for Na-Ion Batteries, J. Electrochem. Soc. 166 (2019) A3723–A3730. https://doi.org/10.1149/2.0721915jes.

[51] J.E. Harlow, S.L. Glazier, J. Li, J.R. Dahn, Use of Asymmetric Average Charge- and Average Discharge-Voltages as an Indicator of the Onset of Unwanted Lithium Deposition in Lithium-Ion Cells, J. Electrochem. Soc. 165 (2018) A3595. https://doi.org/10.1149/2.0011816jes.
[52] G. Yan, R. Dugas, J.-M. Tarascon, The NVPF /Carbon Na-Ion Battery: Its Performance Understanding as Deduced from Differential Voltage Analysis, J. Electrochem. Soc. 165 (2018) A220–A227. https://doi.org/10.1149/2.0831802jes.
[53] A.S. Keefe, S. Buteau, I.G. Hill, J.R. Dahn, Temperature Dependent EIS Studies Separating Charge Transfer Impedance from Contact Impedance in Lithium-Ion Symmetric Cells, J. Electrochem. Soc. 166 (2019) A3272–A3279. https://doi.org/10.1149/2.0541914jes.
[54] J. Landesfeind, J. Hattendorff, A. Ehrl, W.A. Wall, H.A. Gasteiger, Tortuosity Determination of Battery Electrodes and Separators by Impedance Spectroscopy, J. Electrochem. Soc. 163 (2016) A1373. https://doi.org/10.1149/2.1141607jes.
[55] W. Dreyer, J. Jamnik, C. Guhlke, R. Huth, J. Moškon, M. Gaberšček, The thermodynamic origin of hysteresis in insertion batteries, Nature Mater. 9 (2010) 448–453. https://doi.org/10.1038/nmat2730.
[56] A. Criado, P. Lavela, G. Ortiz, J.L. Tirado, C. Pérez-Vicente, N. Bahrou, Z. Edfouf, Highly dispersed oleic-induced nanometric C@Na3V2(PO4)2F3 composites for efficient Na-ion batteries, Electrochimica Acta. 332 (2020) 135502. https://doi.org/10.1016/j.electacta.2019.135502.
[57] N. None, Enabling Fast Charging: A Technology Gap Assessment, EERE Publication and Product Library, Washington, D.C. (United States), 2017. https://doi.org/10.2172/1416167.